L.-W. Hung, Z. A. Jacobson, Z. Ren, A. Javey, and C. T.-C. Nguyen, "Capacitive transducer strengthening via ALD-enabled partial-gap filling," *Tech. Digest*, 2008 Solid-State Sensor, Actuator, and Microsystems Workshop, Hilton Head, SC, June 1-5, 2004, pp. 208-211.

CAPACITIVE TRANSDUCER STRENGTHENING VIA ALD-ENABLED PARTIAL-GAP FILLING

Li-Wen Hung, Zachery A. Jacobson, Zeying Ren, Ali Javey, and Clark T.-C. Nguyen
Department of Electrical Engineering and Computer Sciences
University of California, at Berkeley, CA 94720, U.S.A

ABSTRACT

The electromechanical coupling factors (η_e's) of capacitively-transduced micromechanical resonators have been increased by a factor of 8.1× via a process technology that utilizes atomic layer deposition (ALD) to partially fill the electrode-to-resonator gaps of released resonators with high-*k* dielectric material and thereby achieve effective electrode-to-resonator gap spacings as small as 32 nm. The electromechanical coupling increase afforded by gaps this small not only lowers termination impedances for capacitively-transduced micromechanical filters from the kΩ range to the sub-100Ω range, thereby making them compatible with board-level RF circuits; but does so in a way that reduces micromechanical filter termination resistance R_Q much faster than the electrode-to-resonator overlap capacitance C_o, thereby also substantially increasing the $1/(R_QC_o)$ figure of merit (*FOM*).

INTRODUCTION

To date, capacitively transduced micromechanical resonators have posted the highest *Q*'s of room temperature on-chip resonator technologies, with *Q* values exceeding 200,000 in the VHF range and exceeding 14,600 in the GHz range [1]. This makes them strong candidates for use as RF channel-selectors in next generation software-defined cognitive radios [2], or as ultra-low noise oscillators in high performance radar applications.

Unfortunately, the exceptional *Q*'s of these resonators are not easy to access, because the impedances they present are often much larger than that of the system that uses them. For example, many of today's board-level systems are designed around 50Ω impedance, which is much smaller than the 2.8 kΩ termination resistors required by the 163-MHz differential disk array filter of [3]. Thus, even though the filter of [3] attains an impressively low insertion loss of 2.43 dB for a 0.06% bandwidth, it requires an *L*-network to match to 50Ω. While it is true that as micromechanical filters are integrated together with transistors on single silicon-chips impedance requirements will grow to the kΩ range for best performance [4], off-chip board-level applications will still need lower impedance.

Pursuant to attaining lower capacitive micromechanical resonator impedances, this work employs atomic layer deposition (ALD) [5] to partially fill the electrode-to-resonator gaps of released disk resonators with high-*k* dielectric material and thereby achieve substantially smaller gap spacing, as small as 32 nm. This reduction in gap spacing increases the electromechanical coupling factors (η_e's) of capacitive-transducers by a factor of 8.1×, which not only lowers termination impedances for *capacitively transduced* micromechanical filters from the kΩ range to the sub-100Ω-range, thereby making them compatible with board-level RF circuits; but does so in a way that reduces micromechanical filter termination resistance R_Q much faster than the electrode-to-resonator overlap capacitance C_o, thereby also substantially increasing the $1/(R_QC_o)$ figure of merit (*FOM*). The increase in the FOM is also n^2× faster (hence, better) than that of fully-filled solid-dielectric gap methods for R_x reduction [6]. This partial dielectric-filling based approach further prevents shorting of the resonator to its electrode, hence, greatly improves the resilience of micromechanical resonators against ESD or other events that might pull a resonator into its electrode.

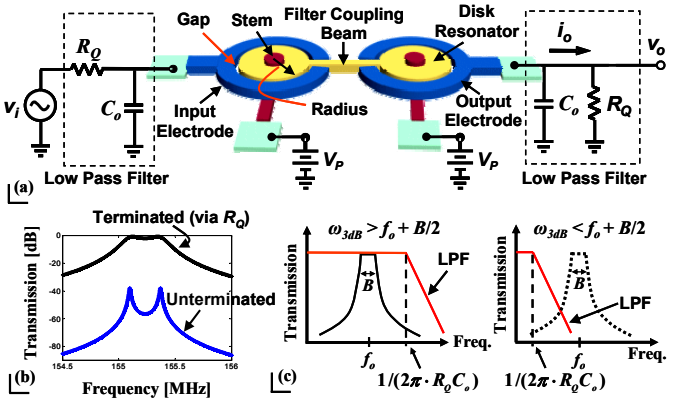

Fig. 1. (a) Perspective-view schematic of a two-resonator micromechanical filter with termination resistors R_Q's and the low-pass filters they form with the C_o's enclosed by dashed lines. (b) Frequency characteristics of an unterminated and a terminated filter with smooth passband. (c) Impact of the low-pass filters in (a) on filter response.

APPROACHES TO IMPROVING FOM

The utility of a $1/(R_QC_o)$ figure of merit is perhaps best conveyed by considering a typical micromechanical filter [3][8], such as shown in Fig. 1, and examining how its termination resistance R_Q and its input capacitance C_o affect its performance. As shown in Fig. 1, the R_Q and C_o essentially combine to generate a pole at $\omega_b = 1/(R_QC_o)$ that sets the 3dB bandwidth of a low-pass filter. If ω_b is lower than the center frequency ω_o of the filter, then it will add undesired passband loss. This problem is actually fixable by using an (on-chip) inductor to resonate out the C_o, but it would be preferable if an inductor were not needed.

The needed value for termination resistance R_Q is given by

$$R_Q = \left(\frac{Q}{qQ_{fltr}} - 1\right) \cdot R_x \approx \frac{Q}{qQ_{filter}} \cdot \frac{m_r \omega_o}{Q\eta_e^2} \approx \frac{m_r B}{q\eta_e^2} \qquad (1)$$

where R_x is the motional resistance of a constituent end resonator, such as shown in Fig. 1; *Q* is the unloaded quality factor of the resonator; $Q_{fltr}=f_o/B$, *B* being the filter passband width; *q* is a normalized parameter obtained from a filter cookbook [7]; m_r is the dynamic mass of the resonator at its point of maximum displacement; and η_e is the electromechanical coupling factor, given by

$$\eta_e = V_P \frac{\partial C}{\partial x} \approx V_P \cdot \frac{A\varepsilon_r\varepsilon_o}{d^2} \qquad (2)$$

where V_P is a dc-bias applied to the conductive resonator structure; $\partial C/\partial x$ is the change in electrode-to-resonator overlap capacitance per displacement; *A* is the electrode-to-resonator overlap area; ε_r is the relative permittivity of the electrode-to-resonator gap material (=1, if not present); ε_o is the permittivity in vacuum; and *d* is the electrode-to-resonator gap spacing.

Using (1)-(2), the expression for figure of merit becomes

Table 1: Comparison of Approaches for R_Q Reduction

Approach	η_e	R_Q	C_o	*FOM*
Arraying with n resonators	$n\times$	$(1/n)\times$	$n\times$	**1×**
Solid-gap filling with $\varepsilon_r=n$	$n\times$	$(1/n^2)\times$	$n\times$	$\boldsymbol{n}\times$
Air gap reduction from d_o to $d=d_o/n$	$n^2\times$	$(1/n^4)\times$	$n\times$	$\boldsymbol{n^3}\times$

$$FOM = \frac{1}{R_Q C_o} \approx \frac{q}{B}\frac{\phi}{\pi}\frac{\varepsilon_o}{\kappa\rho R}\cdot\frac{\varepsilon_r}{d^3} \qquad (3)$$

where ϕ is the angle over which the input electrode subsides; κ is a modifier that accounts for the integration needed to obtain dynamic stiffness [8]; ρ is the density of the disk structural material; R is the radius of the disk (as indicated in Fig. 1); and (3) was reduced to its final form by recognizing that the dynamic mass of the disk at a maximum velocity point on the disk is $m_r = \kappa\rho\pi R^2 t$, where t is thickness.

Of the variables in (3), only ε_r and d are truly adjustable, although R can often be minimized by operating at a fundamental mode, rather than higher modes. This implies that arraying approaches to lowering R_Q [9] that essentially increase the electrode-to-resonator overlap area do not in fact raise the *FOM*. On the other hand, solid-gap filling methods, such as in [6][10], that raise ε_r, do improve the *FOM*, although the improvement ends up being much less than the factor by which ε_r increases, since the need to compress the gap material often greatly reduces the benefits. Thus, it seems to still be gap spacing reduction that provides the largest gain in *FOM*, with very strong third power dependence. In particular, a reduction in gap spacing by 5× yields a 125× increase in *FOM*. Of course, linearity issues will need to be curtailed, as the *IIP3* of the disk will reduce as the gaps shrink [11], but the effects are less consequential as frequencies rise (e.g., at GHz) and can be alleviated in certain mechanical circuit networks.

Table 1 summarizes the efficacy of different approaches to reducing R_Q and increasing *FOM*.

GAP REDUCTION VIA PARTIAL GAP FILLING

Evidently, from an *FOM* perspective, reducing the electrode-to-resonator gap spacing is perhaps the best way to reduce R_Q. Achieving smaller gaps, however, might not be so straightforward. In particular, the process of [3] achieves its sub-100nm lateral gaps using a sacrificial oxide sidewall film that is sandwiched between the resonator and electrode during intermediate process steps, but then removed via a liquid hydrofluoric acid release etchant at the end of the process to achieve the tiny gap. Fig. 2 shows the last step of the fabrication process. Here, sacrificial layers, including sidewall layers, are removed via wet etching to release structures that will eventually move. This approach to achieving lateral gaps, while effective for gap spacings above 50 nm, proves difficult for smaller gap spacings. In particular, smaller gap spacings make it more difficult for etchants to diffuse into the gap and get to the etch front; and for etch by-products to diffuse away from the etch front. While there is some evidence that a gaseous etchant capable of more easily accessing and escaping the gap, such as vapor phase HF, might prove effective for releasing structures with 50nm gaps [12], gaps so small (once released) might be overly susceptible to inadvertent shorting, due to ESD or other catastrophic events.

Rather than removing material by etching, one alternative approach to attaining both sub-50nm high-aspect-ratio gaps and protection against ESD events is to partially fill an already released

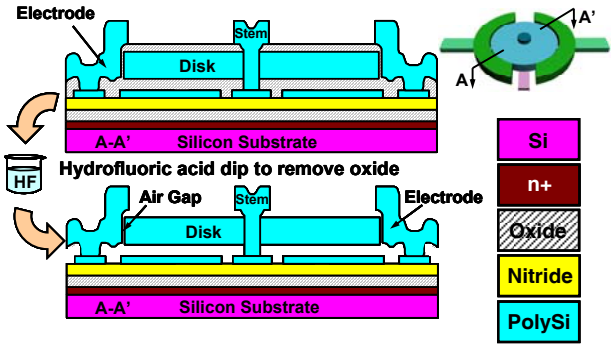

Fig. 2: Cross-sections depicting the final release step in the fabrication sequence for a laterally driven wine-glass disk resonator.

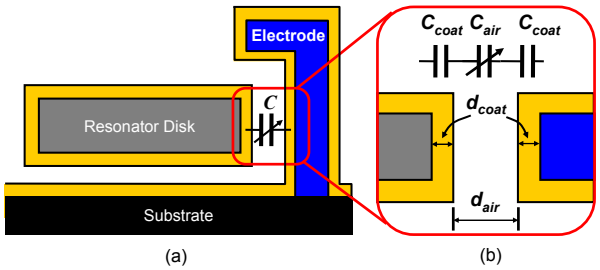

Fig. 3: (a) Schematic of a partial-ALD-filled gap. (b) Enlarged view of the gap and its equivalent series capacitances.

gap with a non-conductive dielectric material, as shown in Fig. 3(a). Here, filling via a dielectric is just as effective as if filling were done with a metal if the permittivity of the dielectric is high enough to allow the air (or vacuum) gap of Fig. 3(b) to set the overall capacitance value. Specifically, the capacitance between the electrode and resonator of Fig. 3(a) can be modeled by the series connection shown in Fig. 3(b). Here, the total electrode-to-resonator capacitance is given by

$$C(x) = C_{coat} \,||\, C_{air}(x) \,||\, C_{coat} = \frac{C_{coat}}{2} \,||\, C_{air}(x) \qquad (4)$$

from which $(\partial C/\partial x)$ can be written (for small x) as

$$\frac{\partial C}{\partial x} = \frac{1}{\varepsilon_o A_o}\left[\frac{C_{coat}}{2} \,||\, C_{air}\right]^2 = \frac{1}{d_{air} C_{air}}\left[\frac{C_{coat}}{2} \,||\, C_{air}\right]^2 \qquad (5)$$

where C_{air} is the capacitance across the air gap for $x = 0$ (i.e. no displacement); $C_{air}(x)$ is this capacitance as a function of displacement x; C_{coat} is the capacitance across each dielectric-coated region; and any dimensions used are defined in Fig. 3. Obviously, if $C_{coat} >> C_{air}$, then the capacitance and $(\partial C/\partial x)$ reduce to

$$C(x) = C_{air}(x) \quad \rightarrow \quad \frac{\partial C}{\partial x} = \frac{C_{air}}{d_{air}} \qquad (6)$$

which are the values that would ensue if there were no dielectric and if the electrode-to-resonator gap were equal to d_{air}. In practice, $C_{coat}/2$ should be at least 10 times larger than C_{air} in order for (7) to hold, which means that the dielectric constant of the filling material should be at least

$$\varepsilon_{coat} \geq 20\varepsilon_o \frac{d_{coat}}{d_{air}} \quad \rightarrow \quad C(x) \cong C_{air}(x) \qquad (7)$$

where the gap dimensions d_{coat} and d_{air} are indicated in Fig. 3. For the case where the gap spacing of a disk resonator is reduced from 94 nm to 32 nm using ALD, achieving a (d_{coat}/d_{air}) ratio of (31/32) and providing a 74 times decrease in R_Q, (7) suggests that the relative permittivity of the dielectric filling material should be >19.4 to allow the use of (7) to determine $(\partial C/\partial x)$; otherwise (6) should be

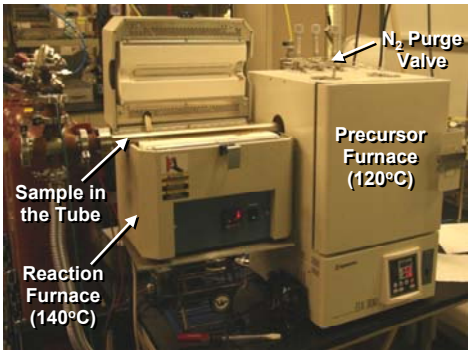

Fig. 4: Photo of the custom-built ALD tool used in this work.

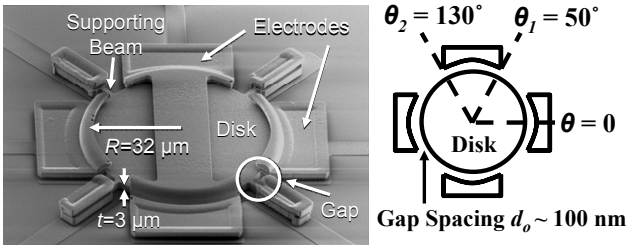

Fig. 5: SEM of a 61-MHz wine-glass disk and some key design parameters.

used. Hafnium oxide (HfO_2) comes close, so is a reasonable choice of dielectric.

EXPERIMENTAL RESULTS

To attain high-aspect-ratio sub-50nm gaps, the starting gap should already be very small, e.g., on the order of 100 nm, so the method used to fill gaps should be very conformal. Recognizing this, atomic layer deposition (ALD) is uniquely adept for this gap-coating process, since its two-step precursor, monolayer-by-monolayer deposition methodology effects very precise film thicknesses with conformality sufficient to uniformly cover the surfaces of the 30:1 aspect ratio 100nm (initial) gaps of the resonators. The post-release process used to reduce gap spacings in this work then consisted merely of an ALD step using a custom-built system (c.f., Fig. 4) to deposit HfO_2 into the gaps of already released disk resonator devices, such as shown in Fig. 5; then a simple lithography and HF dip step to remove HfO_2 over bond pads. The ALD of HfO_2 was done at 140°C using tetrakis (ethylmethylamido) hafnium and water vapor prepared at 120°C.

Fig. 6 presents the measured frequency response characteristics for a 94 nm-gap wine-glass mode disk resonator, with design summarized in Fig. 5, and one coated with 30.7 nm of ALD'ed HfO_2 using the process described above, then sintered in forming gas at 400˚C for 3 minutes (for reasons to be described later). Here, the measured Q of the coated resonator is considerably lower than that of the uncoated one—an observation to be discussed in more detail later. For now, though, accounting for the reduced Q, the extracted η_e's are 19.84 μC/m and 2.44 μC/m at V_P = 16V for the coated and uncoated devices, respectively, yielding an η_e improvement of 8.1×, which is very close to the expected 8.6× difference from (3). The motional resistance R_x at this point is 966 Ω. After another 3 minutes of sintering at 400˚C, the same device achieves R_x=685 Ω and Q = 7,368 at V_P = 19V.

Perhaps the most accurate way to determine the electrode-to-resonator gap spacing for any capacitively transduced resonator is to utilize the dependence of resonance frequency on gap spacing, seen in the expression for resonance frequency

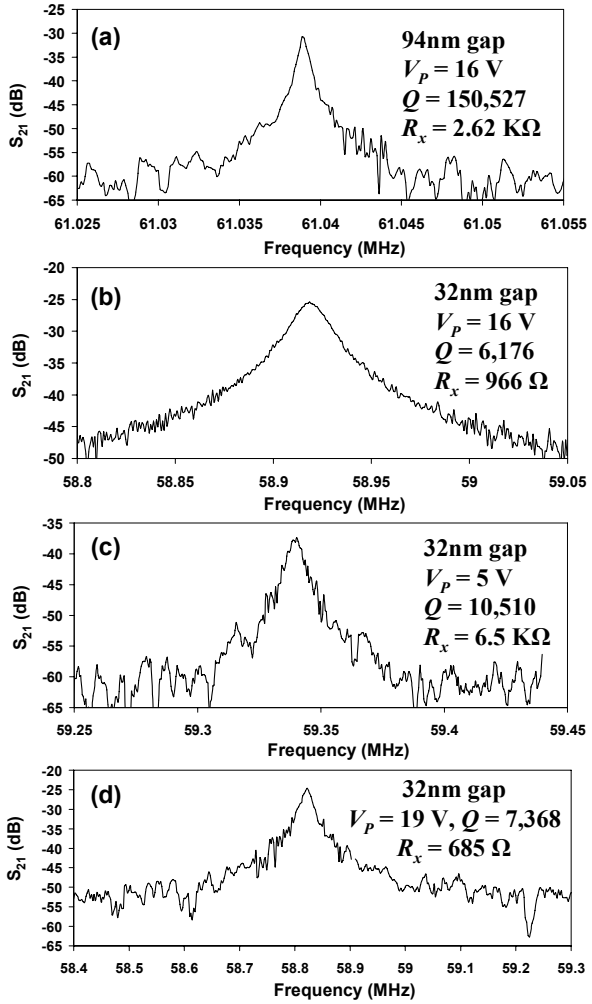

Fig. 6: Frequency characteristics of an initially 94nm-gap resonator before and after ALD coating. From top to bottom: (a) right after HF release; (b) after partially filling the gap with 30.7 nm HfO_2 and sintering at 400˚C for 3 minutes, showing R_x < 1 kΩ; (c) after the same conditions as (b) but with lower V_p, showing Q > 10,000; and (d) after sintering at 400˚C for another 3 minutes, showing even lower R_x at V_P=19V.

$$f_o = \frac{1}{2\pi}\sqrt{\frac{k_m - k_e}{m_r}} = \frac{1}{2\pi}\sqrt{\frac{k_m}{m_r}\left(1 - \left\langle\frac{k_e}{k_m}\right\rangle\right)} \qquad (8)$$

where k_m is the mechanical stiffness, k_e the electrical stiffness, and

$$\left\langle\frac{k_e}{k_m}\right\rangle = \int_{\theta_1}^{\theta_2}\frac{1}{k_m(\theta)}\cdot\left(V_P^{\,2}\frac{\varepsilon_o R t d\theta}{d^2}\right) \qquad (9)$$

where θ_1 and, θ_2 are given in Fig. 5. From (9), the dependence of f_o on V_P is strongly influenced by the gap spacing d_o, suggesting that plots of f_o versus V_P can be used to very accurately extract d_o.

Fig. 7(a) plots frequency versus dc-bias V_P for two devices before and after HfO_2 coating. The data in (a) is for a device different from that of Fig. 6, for which curve-fitting with the theoretical prediction of (8) yields gaps of 97nm for the uncoated disk; and 37 nm for the HfO_2-coated one—both very close to expectations given that ~30 nm of HfO_2 was deposited, all attesting to the precision by which ALD can achieve a specific film thickness. Fig. 7 (b) plots similar measured and theoretical curves for the device in Fig. 6 after HfO_2 ALD, but this time also plotting the theoretical

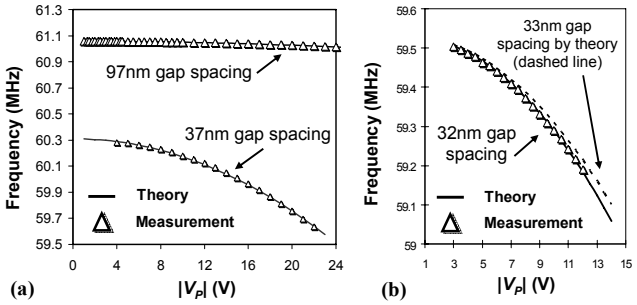

Fig. 7: Resonance frequency f_o vs. dc-bias V_P plots of measurement data and theory (a) a 97nm-gap resonator before and after 30nm HfO_2 coating; and (b) a 32nm-gap partial-filled HfO_2 device.

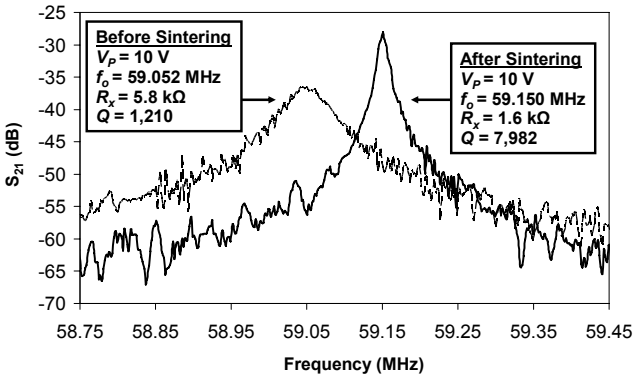

Fig. 8: Frequency characteristic of a 37nm-gap resonator before and after sintering, showing marked improvement in Q.

prediction for a 33nm gap (dashed line). The offset in the curves shows just how sensitive the f_o versus V_P can be in determining d.

Part of the reason for the reduction in Q seen in Fig. 6 derives from the fact that the Q of a resonator with a smaller R_x is loaded more heavily by parasitic interconnect resistance than one with a large R_x. But comparisons of Q versus dc-bias V_P plots suggest that more of the Q reduction seems to derive from surface losses introduced by the HfO_2 film. In this respect, the quality of the HfO_2 deposited film very likely governs the final Q of an ALD-filled device. To gauge to degree to which Q depends upon film quality, ALD-filled devices were sintered at 400˚C in forming gas for varying time periods in order to improve HfO_2 film quality, as done for VLSI transistors [13]. Fig. 8 presents measured frequency characteristics for a 61-MHz wine-glass disk resonator with ALD-coated gaps, showing a marked improvement in Q after 6 minutes of sintering at 350°C. More work is needed to find the best recipe, but it appears that a method to restore Q is at least feasible. It should also be noted that the thicker the ALD coating, the lower the Q of a HfO_2 ALD-coated disk. Thus, another approach to retaining Q's >100,000 for disk resonators is to merely start with a smaller initial gap and deposit a much thinner ALD coating. For example, if the initial gaps were 50 nm, then only 9 nm of ALD would be needed to match the 32 nm gaps of this work, and the Q should be higher.

In addition to Q-reduction, another concern regarding oxide-partial-filled devices is charging. In particular, any charge in the ALD'ed oxide, or at the oxide-silicon interface, will impose a change in electrical stiffness that will pull the frequency of the resonator up or down, according to the sign of the net charge. The existence of such charge is easily discernable by again comparing plots of f_o versus V_P, one with positive V_P, another with the polarity of the V_P reversed (i.e., with V_P = -V_P). Here, a shift in the curve identifies the presence of charge.

Fig. 9 presents plots of f_o versus V_P and reverse polarity V_P for

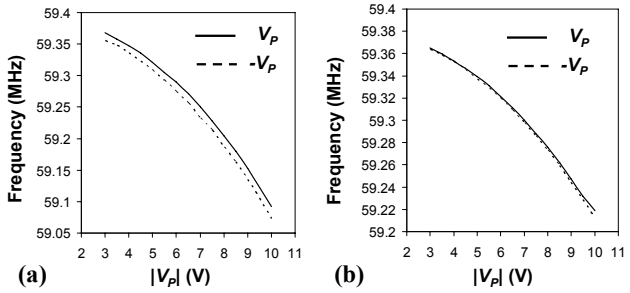

Fig. 9: Resonance frequency f_o vs. dc-bias V_P plots of a 32nm-gap resonator (a) before sintering; and (b) after sintering.

a partial-ALD-filled gap device before and after sintering at 400°C in forming gas for 3 minutes. Before sintering, the curve of positive V_P is horizontally right-shifted from that of negative V_P, while no difference is seen after sintering. It seems that sintering is a very effective means by which to virtually eliminate the oxide charging issue, at least for HfO_2 ALD gap coatings.

CONCLUSIONS

Even with Q reductions caused by partial-ALD-gap filling that in turn result in R_x's only 2.7X better than those of larger air gap devices, the impact of this work is still enormous. This impact is perhaps best gauged by considering the effect of partial-ALD-gap filling on the demonstrated differential disk array filter of [3]. Here, a reduction in gap spacing from 80nm to 32nm of the resonators used in this micromechanical circuit would reduce the needed filter termination resistors R_Q from 2.8kΩ to only 72Ω, which is now compatible with present-day board-level impedances. Since the Q's of the radial-mode disk resonators used in the work of [3] were only 10,500, the Q of 10,510 of this work can maintain the same low insertion loss of 2.43dB for 0.06% bandwidth performance of that filter, but with much smaller matching impedances. Work to actually demonstrate such a filter using partial-ALD-filled gaps is in progress.

Acknowledgment: This work was supported by DARPA.

REFERENCE

[1] S.-S. Li, *et al.*, "Micromechanical "hollow-disk" ring resonators," *Proceedings*, MEMS'04, pp. 821-824.

[2] C. T.-C. Nguyen, "Integrated …," *Proceedings*, Int. Symp. on VLSI Tech., Systems, and Apps., 2008, to be published.

[3] S.-S. Li, *et al.*, "MSI micromechanical differential …," *Tech. Dig.*, Transducers'05, pp. 307-311.

[4] Y. Xie, *et al.*, "1.52-GHz micromechanical …," *IEEE Trans. Ultrason., Ferroelect., Freq. Contr.*, to be published.

[5] D. M. Hausmann, *et al.*, "Atomic layer deposition of hafnium and zirconium oxide …," *Chem. Mater.*, 2002, pp. 4350-4358.

[6] Y.-W. Lin, *et al.*, "Vibrating …," *Proceedings*, IEEE Int. Frequency Control Symposium, 2005, pp. 128-134.

[7] A. I. Zverev, *Handbook of Filter Synthesis*. NY: Wiley, 1967.

[8] F. D. Bannon III, *et al.*, "High-Q HF microelectromechanical filters," *IEEE J. Solid-State Circuits*, vol. 35, no. 4, pp. 512-526, April 2000.

[9] M. Demirci *et al.*, "Mechanically corner-coupled square microresonator array for reduced …," *IEEE/ASME J. Microelectromech. Syst.*, vol. 15, no. 6, pp. 1419-1436, Dec. 2006.

[10] H. Chandrahalim, *et al.*, "Channel-select micromechanical filters using high-k …," *Proceedings*, MEMS'06, pp. 894-897.

[11] R. Navid, *et al.*,"Third-order intermodulation distortion …," *Tech. Dig.*, MEMS'01, Interlaken, Switzerland, Jan. 21-25, 2001, pp. 228-231.

[12] K. Hamaguchi, *et al.*, "3-nm gap fabrication using gas phase sacrificial etching for quantum …," *Tech. Dig.*, IEEE MEMS'04, pp. 418-421.

[13] S. Jeong, *et al.*, "HfO_2 gate insulator formed …," *Thin Solid Films*, vol. 515, pp. 5109.5112, April 2007.